

Numerical Simulation Analysis of Soil Cutting Mechanism Based on CEL Algorithm

Daofa Liu^{1, a}, Yang Liu^{2, b}, Kangjian Shao^{1, c}, Zhengpeng Pu^{1, d}, and Rui Niu^{1, e}

¹ Taihu Laboratory of Deepsea Technological Science Lianyungang Center, Lianyungang, 222006, China, ² Shanghai Branch, China Ship Scientific Research Center (CSSRC), Shanghai, 200011, China.

^a 546533920@qq.com, ^b liuyang@702sh.com, ^c shaokangjian2021@126.com,

^d pulove1998@163.com, ^e niuruihh@163.com.

Abstract. Currently, the understanding of soil cutting mechanisms is still not deep enough, which is not conducive to further optimizing the efficiency and quality of dredging and underwater mining projects. Numerical simulation of tool cutting soil from a three-dimensional perspective using the CEL (Coupled Eulerian Lagrangian) algorithm. In order to further understand the failure mode of soil during actual cutting process and the cutting force of cutting tools, dozens of control working conditions were set up under dynamic cutting soil conditions, and the influence rules of some process parameters involved in the cutting process on the soil cutting operation were analyzed and summarized. The conclusion is that tool width, tool height, cutting speed, and cutting thickness all have a significant impact on the failure mode and cutting force of soil. It is recommended to focus on the influence of these parameters when studying soil cutting related content.

Keywords: Finite element analysis; CEL algorithm; Soil cutting; Numerical simulation

1. Introduction

As the world's dredging, underwater mining engineering and other related industries move towards a higher quality stage, in order to meet the high construction difficulty and high-quality requirements of geotechnical cutting engineering, it is increasingly urgent to develop new geotechnical cutting equipment and propose new construction methods for deep understanding of soil cutting mechanisms. In 1965, Hettiaratchi and Reece[1] first proposed a universal soil pressure model for calculating soil cutting resistance. In 1977, Godwin and Spoor[2] proposed two failure modes of soil based on critical depth when cutting with flat cutting tools. In 1977, McKyes and Ali[3] proposed a three-dimensional soil cutting model. In 1985, Swick and Perumpral[4] proposed a model for quasi-static cutting of soil under the influence of velocity effect. In 1995, Zhang et al.[5] proposed the simple wedge model and the double wedge model for calculating soil resistance. Since the 1980s, Professor Miedema[6-12] and others have conducted extensive research on dredged soil and proposed various mathematical models, which have been widely applied in the field of dredging. Cutting soil with cutting tools is a complex, variable, and nonlinear process. Pure theoretical methods for this problem have limitations and cannot accurately calculate. Therefore, researchers use numerical simulation and experimental methods to study soil cutting. Chen et al.[13] conducted cutting simulations on sand and sandy soil using the discrete element method; Kushwaha et al.[14] used finite element method to numerically simulate the dynamic interaction between clay and tools; Li et al.[15] studied the cutting of clay with flat cutting tools using experimental methods; Su et al.[16] conducted numerical simulation analysis on the cutting of hard clay with flat cutting tools using finite element method. At present, most cutting theories or numerical simulations simulate quasi-static soil cutting while flat cutting tools are running at low speeds; During numerical simulation, there may be significant deformation of the soil during the cutting process, which can lead to non convergence of the calculation; And it can only be applied to specific cutting conditions, such as the inability to accurately calculate the process of cutting soil with high-speed moving tools; Alternatively, using experiments can incur significant economic and time costs. Therefore, in order to shorten time, reduce costs, and maintain a certain level of computational

accuracy, this paper uses finite element method. In order to solve the problem of grid distortion caused by large deformation of soil, CEL method is used for numerical simulation, and multiple working conditions are adopted to be as close as possible to the actual cutting soil conditions. The process of soil cutting under different parameters is studied to deepen the understanding of soil cutting mechanism.

2. Principle Of CEL Method

The CEL algorithm considers factors such as the shape, size, and motion trajectory of an object, and derives the motion equation of the object through the principle of minimum action. The size and shape of an object are described by Lagrangians, which can determine the optimal trajectory of the object during its motion with the smallest Lagrangian. Based on ABQUS software, CEL algorithm is used to simulate the process of soil deformation. The initial state grid of the soil is fixed, penalty function is defined, and contact algorithm is set. The soil is set as an Euler body (the soil material can flow into a mesh cavity without material), and the tool does not deform relative to the soil, so it is set as a Lagrangian body. The cutting of soil materials by cutting tools generates deformation and movement, and the soil materials flow in the grid. Real time calculation of the Euler volume fraction EVF describing the degree of soil occupying the grid can solve the problem of large grid deformation, making the entire calculation process smooth.

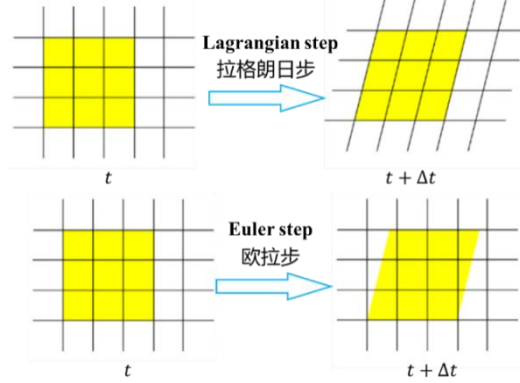


Fig. 1 CEL Algorithm Analysis Steps

In the CEL method, according to the energy conservation law observed by Lagrangian and Euler grids, the time derivative equation in the Lagrangian method is:

$$\frac{D\phi}{Dt} = \frac{\partial\phi}{\partial t} + \mathbf{u} \cdot (\nabla\phi) \quad (1)$$

Mass conservation equation:

$$\frac{D\rho}{Dt} + \rho \nabla \cdot \mathbf{u} = 0 \quad (2)$$

Momentum conservation equation:

$$\rho \frac{D\mathbf{u}}{Dt} = \nabla \cdot \boldsymbol{\sigma} + \rho \mathbf{b} \quad (3)$$

Energy conservation equation:

$$\frac{DE}{Dt} = \nabla \cdot (\boldsymbol{\sigma} \cdot \mathbf{u}) + \rho \mathbf{b} \cdot \mathbf{u} \quad (4)$$

Equation (4) is written in the form of strain rate tensor:

$$\frac{De}{Dt} = \boldsymbol{\sigma} : \mathbf{D} \quad (5)$$

Total energy equation:

$$E = \frac{1}{2} \rho \mathbf{u} \cdot \mathbf{u} + e \quad (6)$$

Under the Euler method, the mass conservation equation:

$$\frac{D\rho}{Dt} + \rho \nabla \cdot \mathbf{u} = 0 \quad (7)$$

Momentum conservation equation:

$$\rho \frac{D\mathbf{u}}{Dt} = \nabla \cdot \boldsymbol{\sigma} + \rho \mathbf{b} \quad (8)$$

Energy conservation equation:

$$\frac{\partial e}{\partial t} + \mathbf{u} \cdot (\nabla e) = \boldsymbol{\sigma} : \mathbf{D} \quad (9)$$

Using the splitting operator for further calculation, the mass, momentum, and energy conservation equations of Euler are:

$$\frac{\partial \rho}{\partial t} + \nabla \cdot (\rho \mathbf{u}) = 0 \quad (10)$$

$$\frac{\partial \rho \mathbf{u}}{\partial t} + \nabla \cdot (\rho \mathbf{u} \otimes \mathbf{u}) = \nabla \cdot \boldsymbol{\sigma} + \rho \mathbf{b} \quad (11)$$

$$\frac{\partial e}{\partial t} + \nabla \cdot (e \mathbf{u}) = \boldsymbol{\sigma} : \mathbf{D} \quad (12)$$

Among them, \otimes represents the tensor product symbol.

For the energy conservation equation under the CEL algorithm, the Lagrangian step is:

$$\frac{\partial \phi}{\partial t} = \mathbf{Q} \quad (13)$$

Euler Step:

$$\frac{\partial \phi}{\partial t} + \nabla \cdot \boldsymbol{\Phi} = 0 \quad (14)$$

Table 1. CEL Algorithm Parameters

Parameter	Symbol	Parameter	Symbol
Solving variables	ϕ	Cauchy stress tensor	$\boldsymbol{\sigma}$
Material point	\mathbf{u}	Physical force	\mathbf{b}
Velocity			
Density	ρ	Total energy per unit volume	E
Source item	\mathbf{Q}	Internal energy per unit volume	e
Flux function	$\boldsymbol{\Phi}$		

3. Numerical model of tool cutting

3.1 Material Settings

The soil material is clay material in the ocean[16]. In order to achieve better numerical simulation results, the Drucker Prager criterion was set as the constitutive model of the soil in ABAQUS software, as shown in Table 2. Due to the much higher hardness of the cutting tool than the soil, it is set as a rigid body and a reference point is set to control the movement of the cutting tool. The material parameters are shown in Table 3.

Table 2. Soil Materials

Parameter	Value	Unit
Elastic modulus	11.088	MPa
Density	1800	kg/m ³
Poisson's ratio	0.19	/
Cohesive force	8.0	kPa
Adhesion force	8.1	kPa
Internal friction angle	2.9	°

Table 3. Tool Material Parameters

Parameter	Symbol	Value	Unit
Density	ρ	7850	kg/m ³
Elastic modulus	E	2.1	GPa
Poisson's ratio	ν	0.3	/

3.2 3D Model And Working Condition Settings

To minimize the influence of boundaries on numerical simulation, the soil model is much larger than the tool. The soil size in the model is 3.5m in length, 2.5m in width, and 1.5m in height, divided into the lower Euler zone and the upper cavity zone.

Tool size: The length is 350mm, the thickness is 20mm, and the width is set according to specific working conditions. The 0-1s time period is the analysis step for geostress balance, and the 1-9s time period is the cutting analysis step.

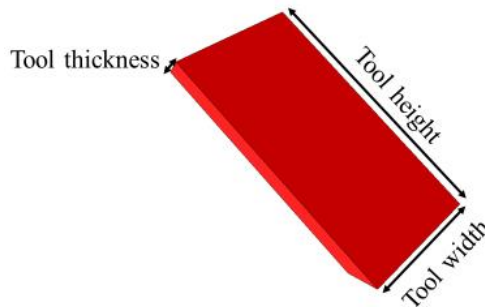


Fig. 1 Tool

The cutting tool is a C3D8 element, and the soil is an EC3D8R8 element. The Euler material zone is used to place soil, while the calculation of the cavity zone initially lacks material. When cutting soil with cutting tools, the soil undergoes deformation and enters the cavity zone. When setting boundary conditions, the faces in the X and Z directions use symmetric boundaries. The bottom of the soil model is completely fixed, the left and right boundaries are fixed in the X-axis direction, the front and rear boundaries are fixed in the Z-axis direction, and the upper surface is a free surface; The tool moves along the negative Z-axis direction.

In order to maintain the accuracy of numerical simulation, five different grid sizes of numerical models were set, and the grid size range of the grid refinement area was set to 10 mm~50 mm. The average cutting force during the stable cutting stage from the 3rd to the 9th second is taken as the evaluation criterion, and the influence of grid size on the numerical simulation results is analyzed. The unchanged parameters include a cutting angle of 60 °, a tool length of 350mm, a cutting thickness of 100mm, and a cutting speed of 0.1 m/s. The change in grid size greatly affects the cutting force of the tool. As the grid gradually decreases, the cutting force tends to converge, and

the smaller the grid, the higher the accuracy. When the grid is 10mm, the cutting force is about 1.03kN, and the number of grids is 1612530; When the grid is 20mm, the cutting force is about 1.39kN, and there are 394272 grids. The difference in cutting force between the two is about 0.36kN, but the number of grids is 4.1 times that of the former. In order to ensure a certain level of accuracy while also considering computational efficiency, the soil mesh size is 20mm in the middle region, and a gradient mesh is set for the rest.

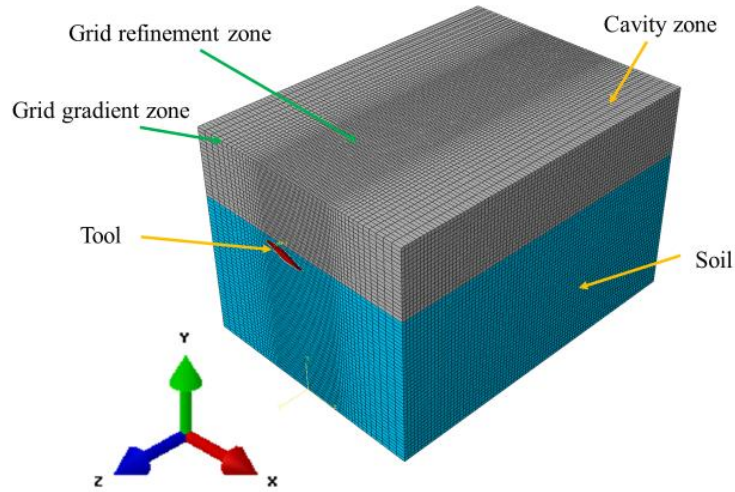


Fig. 3 Numerical Simulation 3D Model

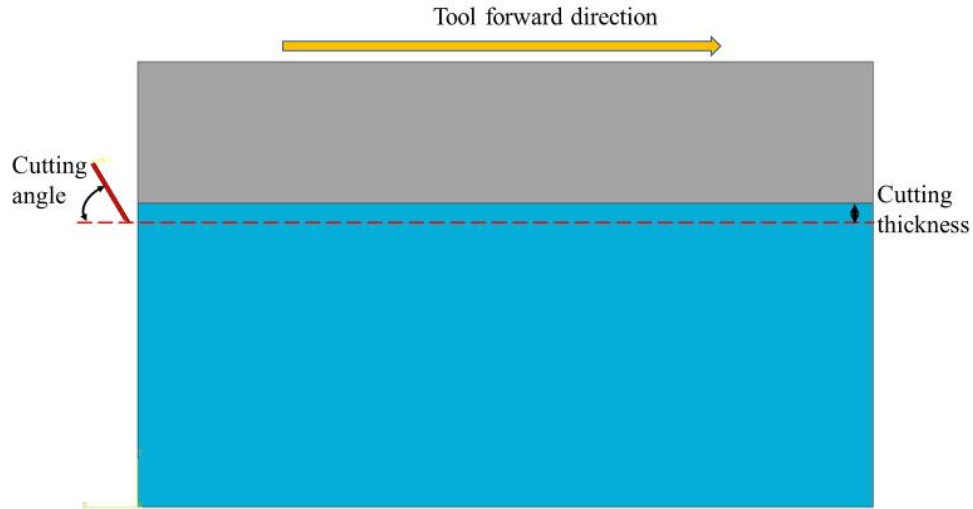


Fig. 4 Schematic diagram of cutting process

Table 4. Setting of Soil Cutting Conditions

Model	Tool width (mm)	Cutting thickness (mm)	Cutting angle ($^{\circ}$)	Cutting Speed (m/s)
1	200	100	60	0.1
2	300	100	60	0.1
3	250	100	60	0.1
4	150	100	60	0.1
5	100	100	60	0.1
6	200	250	60	0.1
7	200	200	60	0.1
8	200	150	60	0.1
9	200	50	60	0.1
10	200	100	90	0.1

11	200	100	75	0.1
12	200	100	45	0.1
13	200	100	30	0.1
14	200	100	60	0.35
15	200	100	60	0.3
16	200	100	60	0.25
17	200	100	60	0.2
18	200	100	60	0.15

Table 5. Model Scheme

Model	Core area grid size (mm)	Number of model grids	Cutting force (kN)
1	10	1612530	1.03
2	20	394272	1.39
3	30	176652	1.65
4	40	110852	1.97
5	50	80262	2.23

4. Numerical Model Of Tool Cutting

4.1 Cutting Process Analysis

Taking the working condition Model-1 as an example, numerical simulations were conducted to obtain the Mises (unit: Pa) stress distribution results at the 2nd, 4th, 6th, and 8th seconds during the soil cutting process under corresponding parameters. From Fig. 5, it can be seen that the tool starts to move forward and comes into contact with the soil. The soil in front of the tool forms a bulge. As the tool further moves, the soil on both sides of the tool gradually separates from the initially formed bulge. During this process, the soil continuously deforms, and finally forms a soil strip that tilts along the tool surface. The area where the tool passes through forms a groove that is the same width as the tool. This phenomenon is similar to the quasi-static cutting experimental results of Rajaram[17]and Zhang et al[18]; During the entire cutting process, the stress bubble continuously increases and the range in the left and right directions is limited. At the separation point between the soil strip and the soil on both sides of the tool, the shear failure stress of the tool is relatively high; Due to compression in front of the soil strip, there is a high stress here, indicating that the soil is only damaged around the cutting tool. In summary, the soil cutting numerical model established in this article can better demonstrate the soil deformation process during the cutting process.

From Fig. 6, it can be seen that during the period of 1-1.8 seconds, due to the slow acceleration of the tool according to the smooth curve, the tool did not initially come into contact with the soil; At 1.8s~2.4s, the tool begins to come into contact with the soil and the soil begins to bulge. As the front boundary is set to be fixed in the Z-axis direction, the cutting force of the tool will change dramatically when it first contacts the soil. During 2.4s~9s, the soil strip has already formed, and the tool's force is stable. The cutting force is in a horizontal straight line state. Therefore, the average value of the cutting force during the 3-9s time period can be taken as the cutting force of the tool. It is obvious that compared to the cutting force in the Z-axis direction, the cutting force in the X-axis and Y-axis directions is smaller, while the cutting force in the Z-axis direction is larger, mainly due to the soil providing greater resistance to the tool in the Z-axis direction. This article will study the cutting force of the cutter based on the total cutting force.

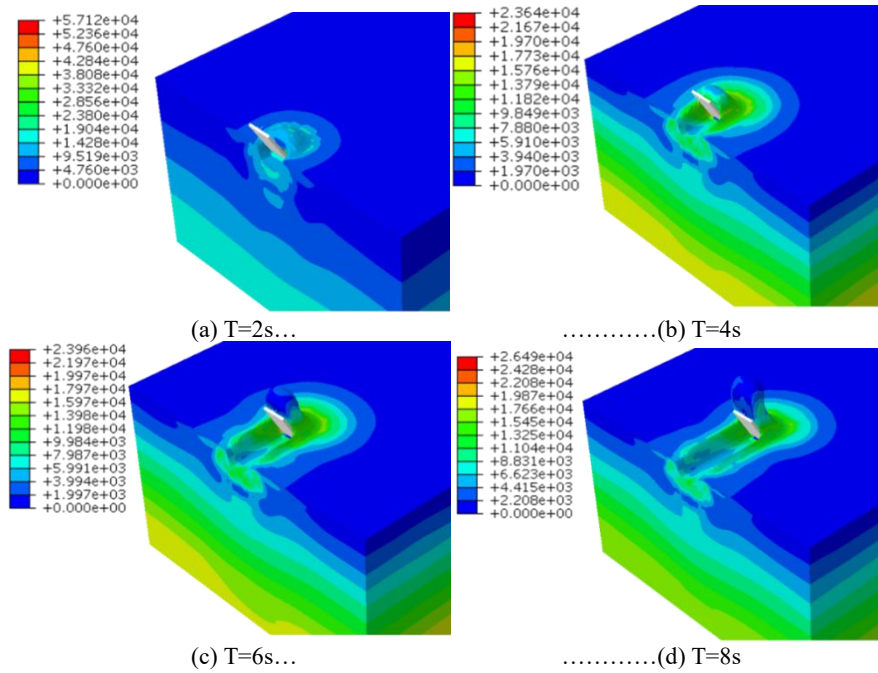


Fig. 5 Mises stress distribution during soil cutting process in Model-1

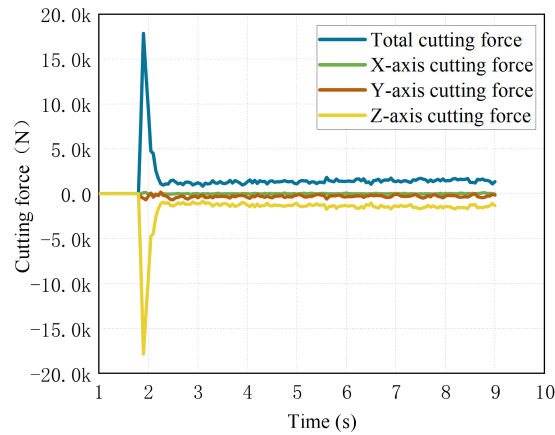
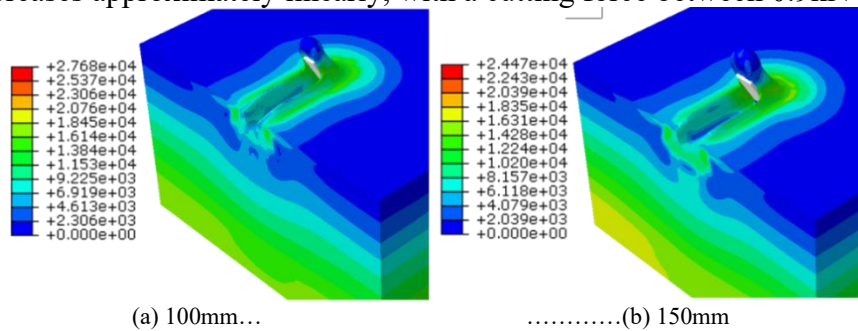


Fig. 6 Tool force in Model-1

4.2 The Influence Of Tool Width

Based on Fig. 7, it can be observed that as the tool width continuously widens, the formed soil strip also widens, and the range of stress bubbles increases, that is, the narrower the tool, the wider the range of soil damage. It can be seen that when the tool width is greater than 150mm, the soil strip shows a bent state; When the tool width is less than or equal to 150mm, the soil strip has almost no bending. From Fig. 8, it can be seen that as the width of the cutting tool increases, its cutting force increases approximately linearly, with a cutting force between 0.9kN and 1.8kN.



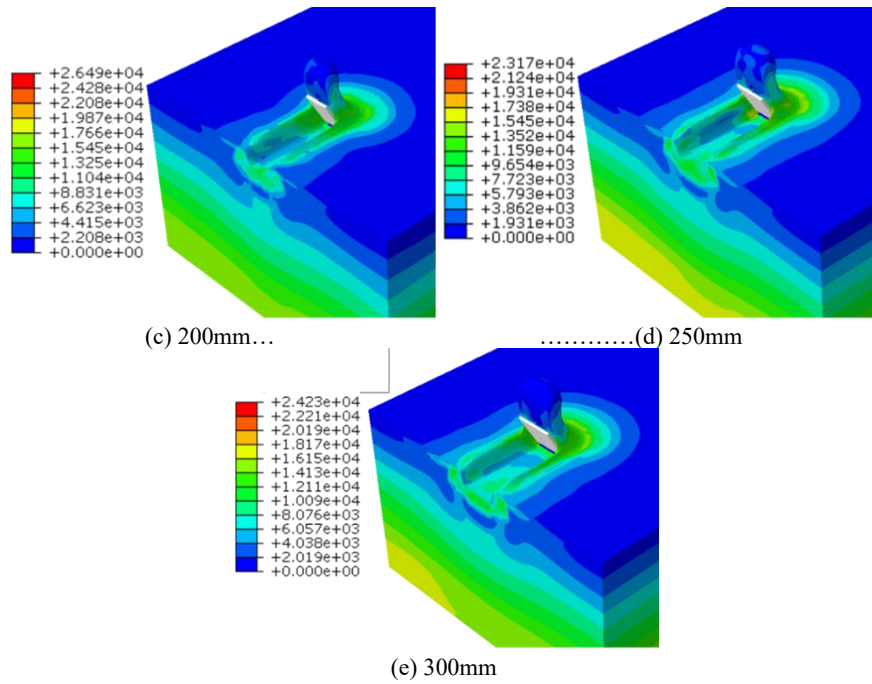


Fig. 7 Mises stress distribution under different tool widths

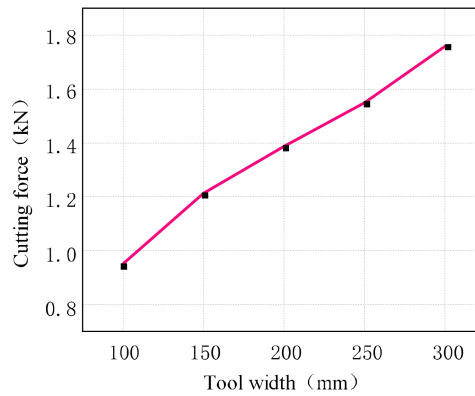


Fig. 8 Cutting forces with different tool widths

4.3 The Influence Of Cutting Thickness

From Fig. 9, it can be seen that as the cutting thickness increases, the thickness of the soil strip also increases, and the degree of adhesion between the side of the soil strip and the soil increases. Finally, when the thickness reaches 250mm, the soil strip does not separate from the soil, forming a tunnel shape. At the same time, the range of stress bubbles gradually expands, and the range of damage to the soil increases, but the cutting effect decreases after reaching a certain thickness. From Fig. 10, it can be observed that as the thickness of the soil layer being cut increases, the cutting force also increases, with a cutting force range of 0.9kN to 5.1kN. When the cutting thickness is between 50-100mm, the change in cutting force is small. When it is greater than 100mm, due to the increased connection between the soil strip side and the soil, and the increased contact area between the Z-axis direction of the tool and the soil, the degree of change in cutting force is large.

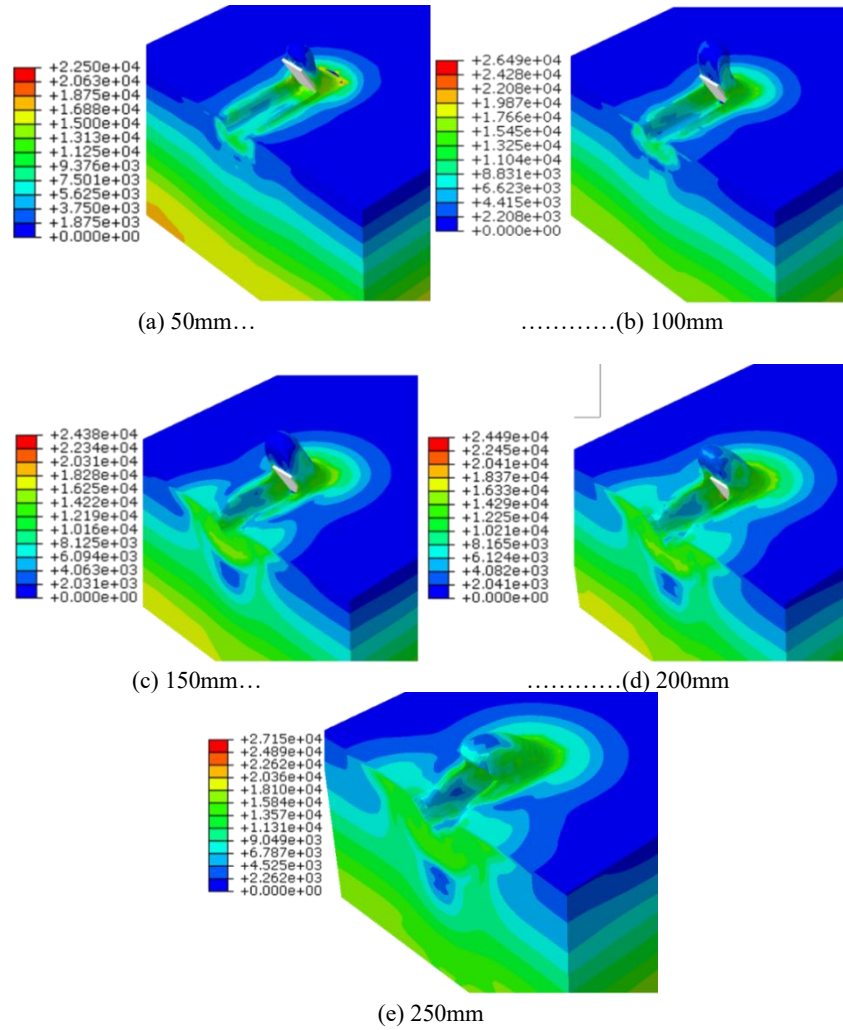


Fig. 9 Mises stress distribution under different cutting thicknesses

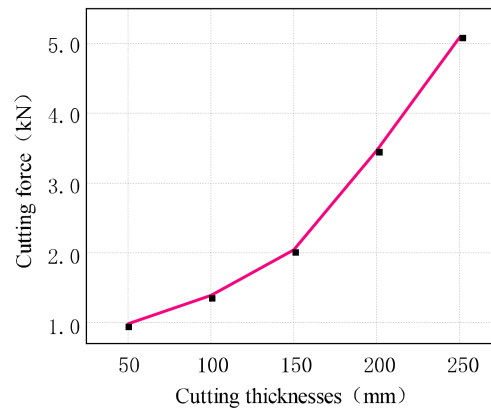


Fig. 10 Cutting force under different cutting thicknesses

4.4 The Influence Of Cutting Angle

From Fig. 11, it can be seen that as the cutting angle increases, at 45° , the soil strip gradually forms, the thickness of the soil strip increases, and the range of stress bubbles also gradually increases. When the cutting angle is 75° , the stress at the connection between the soil below and the soil is maximum. From Fig. 12, it can be seen that when the cutting angle is between 30° and 60° , the cutting force first increases and then decreases; Between 60° and 90° , the cutting force increases with the increase of cutting angle, and the degree of change gradually increases. When the cutting angle is 30° and 60° , the cutting force is at a relatively small level of about 1.4kN; When

the cutting angle is 90° , the cutting force reaches its maximum, with a magnitude of approximately 2.0kN.

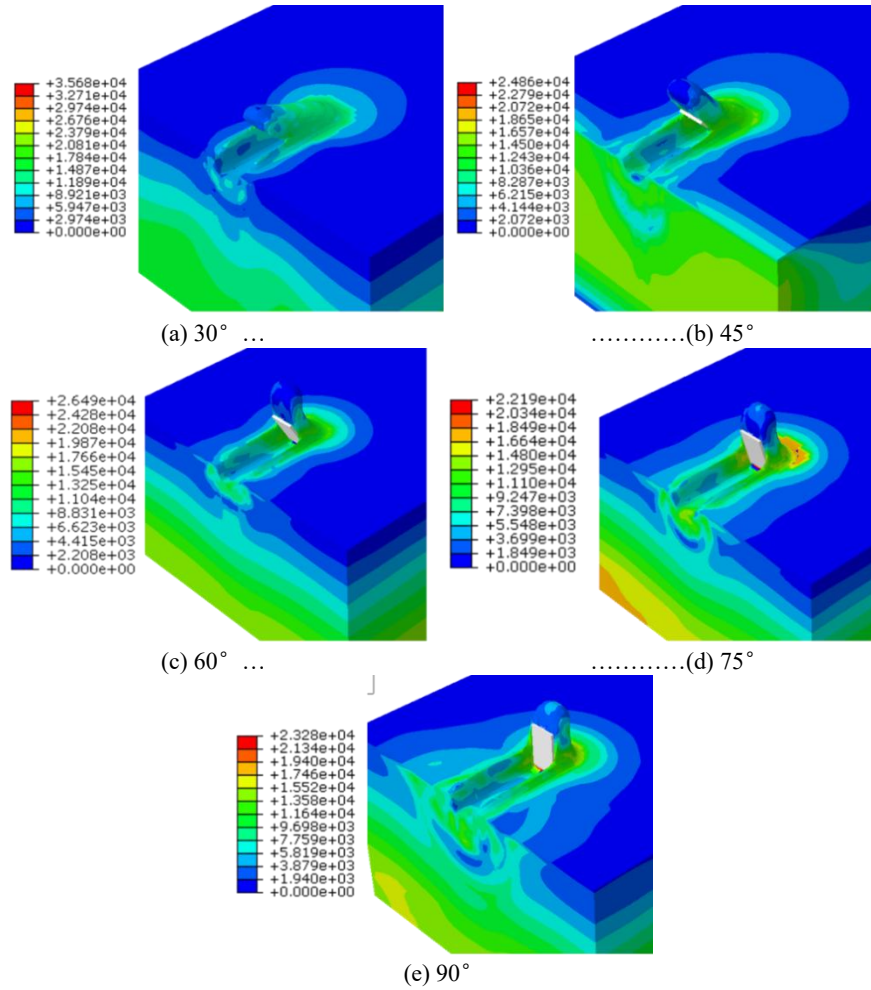


Fig. 11 Mises stress distribution at different cutting angles

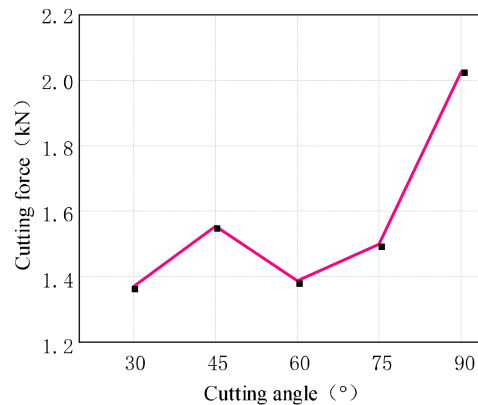


Fig. 12 Cutting force at different cutting angles

4.5 The Influence Of Cutting Speed

As shown in Fig. 13, with the increase of cutting speed, the length of the soil strip also becomes longer, forming a crescent shape along the direction of tool guidance,. The range of stress bubbles is basically near the soil groove and around the soil strip. When the cutting speed is greater than 0.1m/s, this phenomenon can be clearly observed. As shown in Fig. 14, with the increase of tool speed, the cutting force curve approximately shows a linear increase. When the cutting speed is between 0.1~0.35m/s, the range of cutting force is 1.3kN~1.8kN.

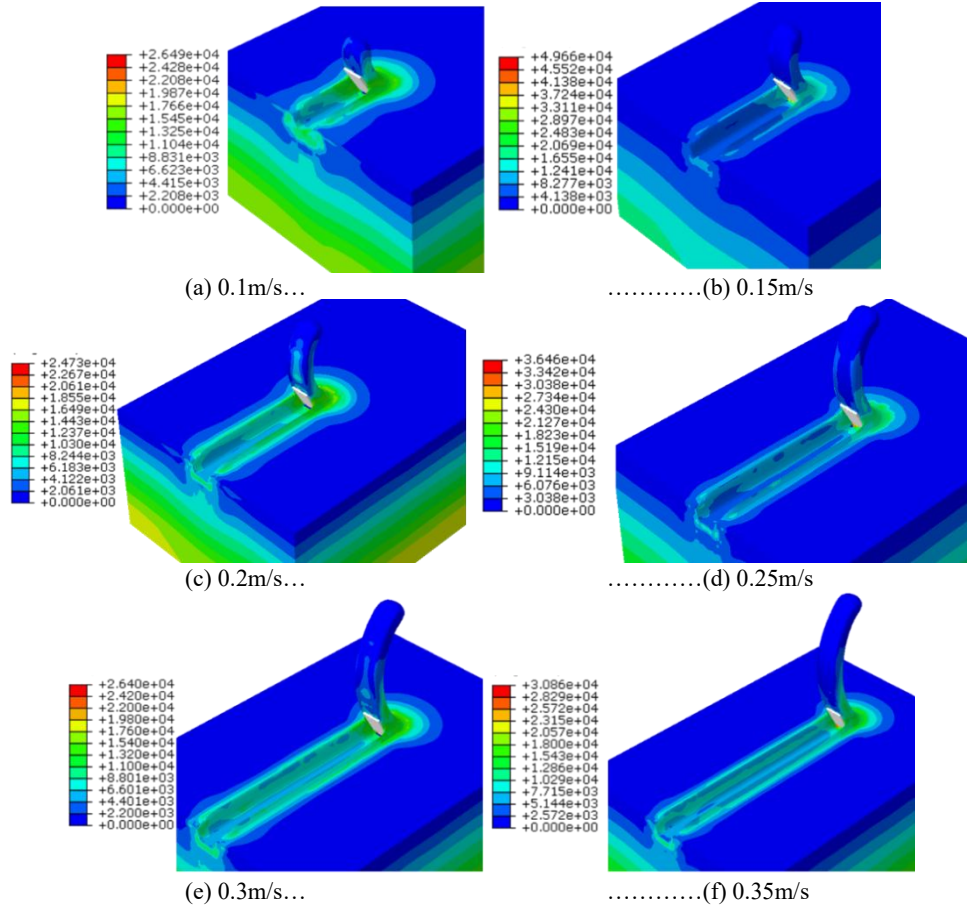


Fig. 13 Mises stress distribution under different cutting speeds

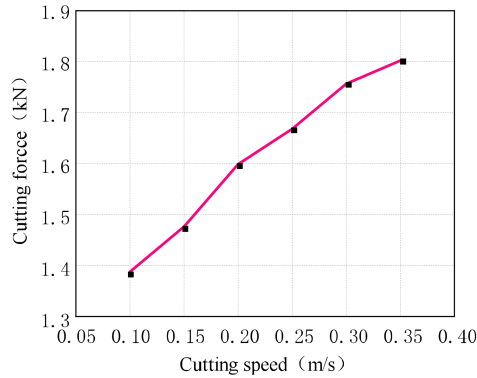


Fig. 14 Cutting force at different cutting speeds

5. Summary

This article uses the CEL algorithm to numerically simulate the cutting of soil by flat cutting tools, and sets up multiple sets of working conditions for comparative analysis. The changes in tool width, tool height, cutting speed, and cutting thickness all have a significant impact on the failure mode and cutting force of soil, and the following conclusions are drawn:

(1) In ABAQUS software, the CEL algorithm can accurately simulate the process of tool cutting soil, more intuitively display the failure mode of soil under different working conditions, and the cutting force of the tool, providing a basis for a deeper understanding of the deformation mechanism of tool cutting soil.

(2) During the numerical simulation process, the soil in front of the tool will gradually bulge and form soil strips. In this process, the cutting force curve changes significantly before the contour of

the soil strip is formed. After the soil is formed, the cutting force curve reaches a stable state and basically follows a horizontal straight line.

(3) Under dynamic cutting conditions, the tool widens, the soil strip widens, and the cutting force increases linearly; As the cutting thickness increases, the soil strip becomes thicker, and the amplitude of cutting force changes accordingly, resulting in an increase in the magnitude of cutting force; When the cutting angle is between 30° and 90° , the cutting force first increases and then decreases with the cutting angle, and then increases again; The soil strip becomes longer and the cutting force increases with the increase of cutting speed.

References

- [1] Hettiaratchi, D.R.P., A.R., The calculation of passive soil resistance[J]. *Geotechnique* 1965(3), 289--310 .
- [2] Godwin R J, Spoor G. Soil failure with narrow tines[J]. *Journal of Agricultural Engineering Research*, 1977, 22(3): 213-228.
- [3] McKyes E, Ali O S. The cutting of soil by narrow blades[J]. *Journal of Terramechanics*, 1977, 14(2): 43-58.
- [4] Swick W C, Perumpral J V . A model for predicting dynamic soil tool interaction[J]. *Journal of Terramechanics*, 1985, 22(3):175-175.
- [5] Zhang J I, Kushwaha R L. A modified model to predict soil cutting resistance[J]. *Soil and Tillage Research*, 1995, 34(3): 157-168.
- [6] Miedema S. The Delft Sand, Clay & Rock Cutting Model 3rd Edition[M]. Amsterdam, The Netherlands: Delft University Press / IOS Press, 2019.
- [7] Miedema S A. Mathematical Modelling of the Cutting of Densely Compacted Sand Under Water[J]. *Dredging & Port Construction*, 1985, 7: 22-26.
- [8] Miedema S A. Calculation of the cutting forces when cutting water saturated sand[J]. Doctor thesis, Delft, Netherlands, 1987.
- [9] Miedema S A. On the Cutting Forces in Saturated Sand of a Seagoing Cutter Suction Dredge[J]. *Proc. WODCON XII*, Orlando, USA, 1989.
- [10] Miedema S A, Frijters D. The Mechanism of Kinematic Wedges at Large Cutting Angles-Velocity and Friction Measurements[C]//23rd WEDA Technical Conference & 35th TAMU Dredging Seminar, Chicago, USA. 2003.
- [11] He J, Miedema S A, Vlasblom W J. FEM Analyses Of Cutting Of Anisotropic Densely Compacted and Saturated Sand[J]. *WEDAXXV & TAMU37*, New Orleans, USA, 2005.
- [12] Miedema S A. New developments of cutting theories with respect to dredging, the cutting of clay and rock[J]. *WEDA XXIX & Texas A&M*, 2009, 40: 14-17.
- [13] Chen Y, Munkholm L J, Nyord T. A discrete element model for soil-sweep interaction in three different soils[J]. *Soil and Tillage Research*, 2013, 126: 34-41.
- [14] Kushwaha R L, Shen J. Finite element analysis of the dynamic interaction between soil and tillage tool[J]. *Transactions of the ASAE*, 1995, 38(5): 1315-1319.
- [15] LIZhang-chao, ZHANG Geng-sheng, XIAO Bo. Experimental study on mechanism of clay cutting by single rake tooth[J]. *Port & Waterway Engineering*, 2020, (S1):85-90.
- [16] SU Zhao-bin, CHEN Jiu-xiao. Finite element simulation for cutting process of hard clay in Tianjin Port area [J]. *Port & Waterway Engineering*, 2022, (01):173-178.
- [17] RAJARAM G, GEE-CLOUGH D. Force-distance behaviour of tine implements[J]. *Journal of Agricultural Engineering Research*, 1988, 41(2): 81-98.
- [18] Lingbo Zhang. Research on numerical simulation of cutting of soft rock and clay with plane tine cutters [D]. Tianjin: Tianjin University, 2018.